ACS OMEGA

http://pubs.acs.org/journal/acsodf

Article

Application of Circular Dichroism and Fluorescence Spectroscopies To Assess Photostability of Water-Soluble Porcine Lens Proteins

Claudia Honisch, Viola Donadello, Rohanah Hussain, Daniele Peterle, Vincenzo De Filippis, Giorgio Arrigoni, Claudio Gatto, Laura Giurgola, Giuliano Siligardi, and Paolo Ruzza*

Cite This: *ACS Omega* 2020, 5, 4293−4301

Read Online

ACCESS | Metrics & More | Article Recommendations | Supporting Information

ABSTRACT: The eye lens is mainly composed of the highly ordered water-soluble (WS) proteins named crystallins. The aggregation and insolubilization of these proteins lead to progressive lens opacification until cataract onset. Although this is a well-known disease, the mechanism of eye lens protein aggregation is not well understood; however, one of the recognized causes of proteins modification is related to the exposure to UV light. For this reason, the spectroscopic properties of WS lens proteins and their stability to UV irradiation have been evaluated by different biophysical methods including synchrotron radiation circular dichroism, fluorescence, and circular dichroism spectroscopies. Moreover, dynamic light scattering, gel electrophoresis, transmission electron microscopy, and protein digestion followed by tandem LC−MS/MS analysis were used to study the morphological and structural changes in protein aggregates induced by exposure to UV light. Our results clearly indicated that the exposure to UV radiation modified the protein conformation, inducing a loss of ordered structure and aggregation. Furthermore, we confirmed that these changes were attributable to the generation of reactive oxygen species due to the irradiation of the protein sample. This approach, involving the photodenaturation of proteins, provides a benchmark in high-throughput screening of small molecules suitable to prevent protein denaturation and aggregation.

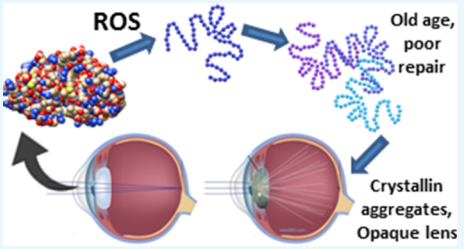

1. INTRODUCTION

The crystalline lens is a transparent, elastic, avascular organ that allows refracting light to focus objects on the retina.[1] Besides the accommodation of objects on the retina, crystalline lens protects the retina from the damage of ultraviolet light.[2] The lens high transparency and refraction are due to the lack of organelles within the mature lens fiber cells and to the highly ordered structure of the water-soluble (WS) proteins called crystallins.[3−5]

Crystallins are present at an extraordinary high concentration, up to 450 mg/mL, in the eye lens and are essential for the maintenance of lens transparency and refraction.[6] The structural stability and solubility of crystallins, enhanced by protein interactions, is important to lens transparency since they last a lifetime with virtually no protein turnover.[7] Indeed, at a high protein concentration, crystallins repel each other and form short-range interactions in a dense liquid or glass-like structure, which allows the homogeneity of the refractive index inside the single mature lens fiber cells.[6] Despite this homogeneity, a gradient of refractive index in the crystalline lens from approximately 1.406 in the central layers down to 1.386 in the less dense cortex has been detected,[8,9] which contributes to the correction of the spherical aberration of the lens so that light can focus onto the retina with minimal scattering.[10]

Three groups of mammalian soluble lens proteins, named α-, β-, and γ-crystallins, are identified and isolated according to their molecular weight.[6,8−10] Notably, although present in different forms of aggregation, all α-, β-, and γ-crystallin monomers have a similar molecular mass of approximately 20 kDa.[11]

α-Crystallin makes up about 40% of eye lens proteins. It exists as a large aggregate of approximately 800 kDa composed of two subunits, αA- and αB-crystallin, which adopt a spherical structure with an internal cavity.[12] Aside from its role in sustaining the refractive index, α-crystallin plays an important role in preventing the formation of aggregates that can scatter the light.[13] Indeed, α-crystallin is a molecular chaperon that protects eye lens proteins from detrimental protein aggregation by binding to partially unfolded proteins, maintaining them in a refolding-competent state, minimizing the size of the nucleating species, and inhibiting their further growth.[14]

β- and γ-crystallins belong to the $\beta\gamma$-superfamily that has evolved from a common primordial source.[15] This superfamily is more heterogeneous, and different isoforms of these proteins have been identified. β-Crystallins are identical to γ-crystallins in structure and play an important role in the maintenance of the lens refractive index. Unlike γ-crystallins, β-crystallins have

Received: December 10, 2019
Accepted: February 4, 2020
Published: February 17, 2020

https://dx.doi.org/10.1021/acsomega.9b04234
ACS Omega 2020, 5, 4293−4301

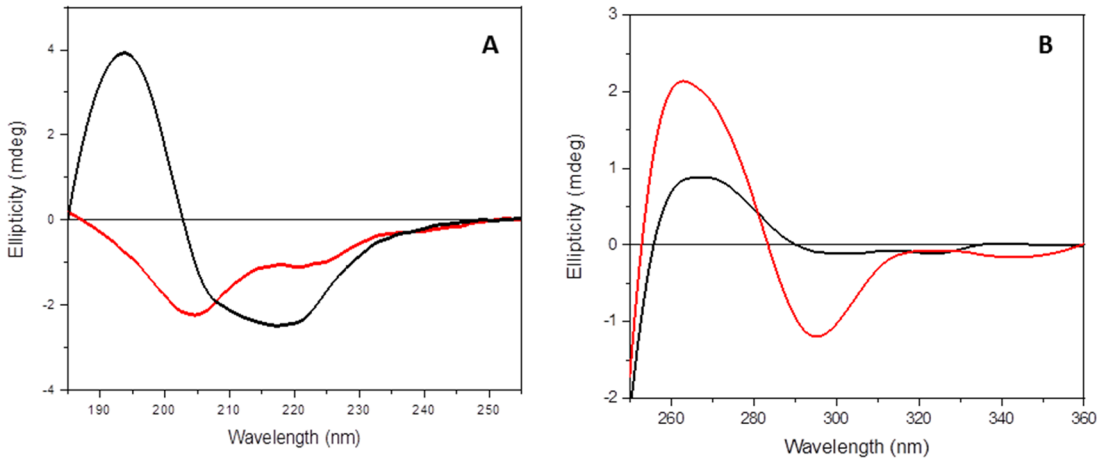

Figure 1. CD spectra of WS proteins isolated from pig lenses before (black) and after (red) exposure to UV-C light (254 nm). (A) Far-UV CD spectra of WS proteins (0.09 mg/mL) in 10 mM phosphate buffer, pH 7.2, measured with a Jasco J-1500 spectropolarimeter. Conditions: response of 1 s, data pitch of 0.5 nm, 1.0 nm bandwidth, and 0.1 cm path length cell (200 μL). (B) Near-UV CD spectra of WS proteins (0.09 mg/mL) in 10 mM phosphate buffer, pH 7.2, measured with a Jasco J-1500 spectropolarimeter. Conditions: response of 1 s, data pitch of 0.5 nm, 1.0 nm bandwidth, and 0.1 cm path length cell (200 μL).

various forms of homomers and heteromers and become easily denatured both thermally and chemically.[16] The $\beta\gamma$-superfamily is structurally characterized by the presence of two Greek key motifs[17−20] consisting of four-stranded antiparallel β-sheet structures. The relative position of these domains in crystallins differs, having two different conformations referred as either "closed" or "opened", respectively.[21] It has been suggested that an opened conformation forces crystallins to favor intermolecular domain interactions characteristic of oligomers compared with intramolecular contacts present in a closed conformation characteristic of monomeric crystallins.

The aggregation and insolubilization of crystallins cause the degeneration and opacification of crystalline lens, inducing the formation of cataract.[22−24] Although this disorder is a well-known disease, the mechanism of eye lens protein aggregation is not well understood. This abnormal aggregation is considered to be triggered by various post-translational modifications that have been described in many reviews.[25−27] Among the possible causes of these modifications, the action of free radicals and reactive oxygen species (ROS) generated by UV radiation has been found.[28] Indeed, UV radiation is considered one of the factors responsible for oxidative changes in lens proteins with age and in cataract onset.[29,30] However, protein structural changes due to UV irradiation so far has not been well identified. Here, we aim to show the protein aggregation mechanism by UV irradiation initialized by the ROS formation.

Structural and mechanistic studies performed on γD- and αB-crystallins demonstrated that these proteins can form amyloid fibers when aggregated. Indeed, γD-crystallin forms amyloid fibers when denatured by acid, while it precipitates as both disordered aggregates and amyloid fibers upon UV irradiation.[31−34] On the other hand, αB-crystallin forms an amyloid structure when incubated at 60 °C in the presence of 10% TFE.[35]

Recently, we demonstrated that the high photon flux and brilliance of synchrotron radiation can induce protein denaturation when repeated consecutive synchrotron radiation circular dichroism (SRCD) spectra are acquired in the far-UV region and that this phenomenon can be used to study the effects of ligand and medium composition on protein stability.[36−38] Moreover, studies performed in the presence of the positive ROS fluorescent probe dihydrorhodamine-123 (DHR-123) demonstrated that ROSs have been produced in a water solution exposed to either synchrotron radiation or UV-C light (254 nm), indicating the involvement of these species in the protein denaturation (personal communication).

With the aim to study the spectroscopic properties of water-soluble lens proteins and the conformational changes due to their exposure to UV light, we isolated the water-soluble (WS) protein fraction from porcine lenses, which was analyzed by biophysical techniques including SRCD, fluorescence, and circular dichroism (CD) spectroscopies. While previous studies were conducted on single crystallin protein isoforms, in this work, the total water-soluble fraction was used, permitting to evaluate the protective and/or cooperative contribute of each protein on the misfolding and aggregation process. The use of SR exposure as a tool to trigger UV denaturation is a novel methodology in this field. Our results clearly indicated that the exposure to UV light strongly modified the protein conformation, inducing their aggregation with a mechanism mediated by ROS.

2. RESULTS AND DISCUSSION

2.1. Isolation and Characterization of Water-Soluble Lens Proteins. The water-soluble fraction (WS) of porcine lens proteins was extracted from young healthy animal lenses and characterized by both SDS-PAGE and LC−MS/MS. Electrophoretic analysis (Figure S1) shows that, under non-reducing conditions, the molecular weight distribution of this fraction is in the 17−47 kDa range. Under reducing conditions, the electrophoretic separation pattern simplifies, showing the presence of the four-band pattern corresponding to the classical crystallin protein profile in the 17−25 kDa molecular weight range, while the protein band at 48 kDa disappears, indicating the presence of a dimeric structure.

LC−MS/MS analysis of the tryptic digest (Table S1 in the Supporting Information) identifies the presence of tryptic fragments with a mass and sequence corresponding to that of α-, β-, and γ-crystallin proteolytic products, indicating the presence of these proteins in the WS fraction.

https://dx.doi.org/10.1021/acsomega.9b04234
ACS Omega 2020, 5, 4293−4301

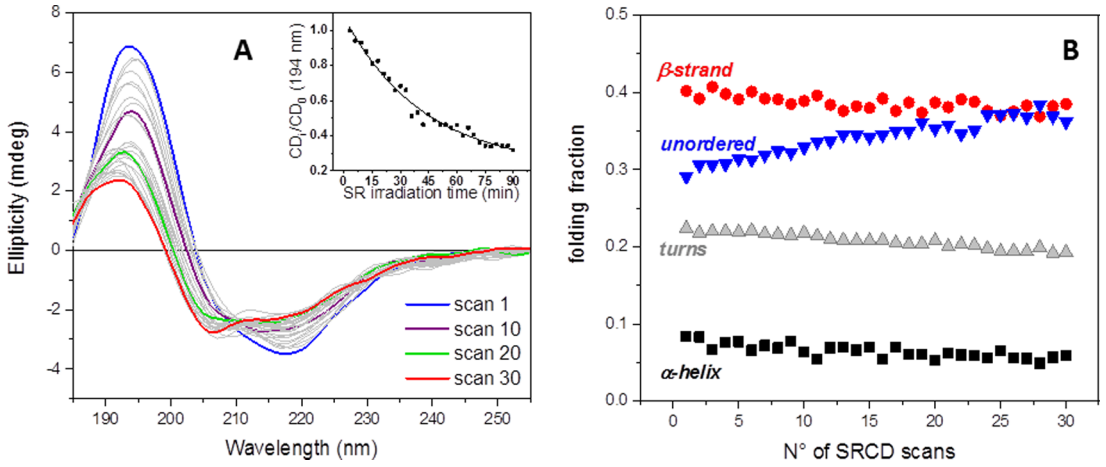

Figure 2. WS proteins SRCD UV-denaturation assays. (A) Thirty repeated consecutive SRCD scans of WS proteins (0.45 mg/mL) in 10 mM phosphate buffer solution, pH 7.2, measured with B23 module B. SR irradiation time is indicated in the legend. The solid black line indicates the first scan and the solid red line the 30th scan. Conditions: integration time of 1 s, 0.02 cm path length cell (60 μL), and monochromator bandwidth of 1.8 nm. (B) Plot of the secondary structure component change during the experiment (α-helix in black, β-strand in red, unordered in blue, and turns in gray).

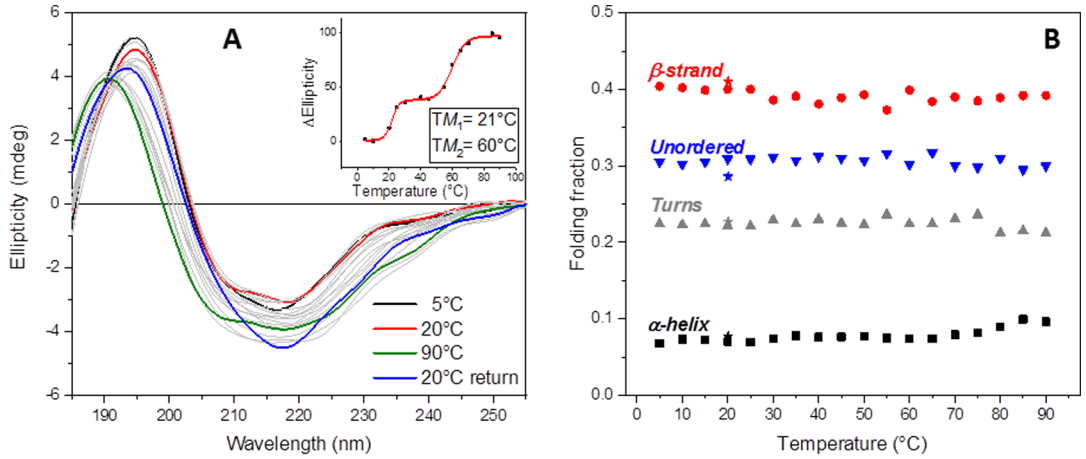

Figure 3. WS proteins thermal denaturation assay. (A) Far-UV SRCD spectra of WS proteins (0.45 mg/mL) in 10 mM phosphate buffer solution, pH 7.2, measured with B23 module B at different temperatures. Conditions: integration time of 1 s, 0.02 cm path length cell (60 μL), and monochromator bandwidth of 1.2 nm. Inset: melting curves of WS proteins constructed plotting the SRCD ellipticity at 194 nm versus temperature.(B) Plot of secondary structure component change during the experiment (α-helix in black, β-strand in red, unordered in blue, and turns in gray; stars represent the structure at 20 °C recorded after the heating process).

2.2. Circular Dichroism Spectroscopy. The far- and near-UV CD spectra of WS proteins are reported in Figure 1. The far-UV CD spectrum (Figure 1A) is characterized by the presence of a positive band at 194 nm and a negative band at about 215 nm, indicative of a predominant β-strand secondary structure.[39] The near-UV CD spectrum shows a positive band at about 265 nm that includes the contribute of disulfide groups and a negative band at about 295 nm due to the L_b transition[40,41] of aromatic side chain residues (Figure 1B).

The exposure to UV-C radiation for 45 min profoundly modified the CD spectra in both the examined UV regions. The bands at 194 and 215 nm, characterizing the far-UV CD spectrum, disappeared, replaced by a negative band at 205 nm with a shoulder at about 222 nm, suggesting the presence of a predominant unordered conformation (Figure 1A) as confirmed by the estimation of the secondary structure (Figure S1 in the Supporting Information). Moreover, in the near-UV CD spectrum, the negative band at 295 nm disappeared, while the intensity of the positive band at 265 nm strongly decreased (Figure 1B), confirming the disruptive effect of the exposure to UV-C light on the protein conformation.

This effect, in a diluted protein solution, is the result of two different mechanisms, which both induce the formation of ROS. The first is due to the photolysis of solvent (water) molecules present in large concentration (about 55 M)[42] with the generation of the hydroxyl radical $^{\cdot}$OH and the superoxide anion radical $O_2^{\cdot-}$,[42,43] which can react with different protein targets including aromatic residues, methionine, cysteine, and disulfide bonds. The latter mechanism involves a direct interaction of UV light with protein chromophores that can capture the UV radiation forming excited states able to transfer an electron to nearby groups or to give radical anions via hydrated electrons formation,[44] disrupting the secondary structure of proteins.

2.3. Synchrotron Radiation Circular Dichroism Spectroscopy. The high photon flux and brilliance of the synchrotron radiation of the Diamond Light Source synchrotron allow the direct investigation of the WS lens protein

https://dx.doi.org/10.1021/acsomega.9b04234
ACS Omega 2020, 5, 4293−4301

denaturation mediated by UV-light by acquiring consecutive repeated SRCD spectra in the far-UV region. Indeed, it has been demonstrated that a photodenaturation of ordered proteins occurs when consecutive repeated scans were collected,[36,38,45] and that this is essentially due to the generation of free radicals (personal communication).

To this purpose, 30 consecutive repeated scans in the 185−260 nm region were collected (Figure 2A). A drastic change in the far-UV SRCD spectrum of the WS protein fraction was detected after 30 scans, and the analysis of the secondary structure content indicated an increase in the unordered structure content from 30 to 35% to which corresponds a decrease in the β-strand content (from 39 to 36%) and, more generally, in the ordered structure content (Figure 2B) likewise observed in the UV-C irradiation experiments.

To exclude an effect related to a local heating, comparative thermal stability experiments in the 5−90 °C range were performed (Figure 3A). After heating, only a small decrease (less than 20%) in the intensity of the CD bands was observed, while no difference in the shape of the spectrum was detected. Moreover, the secondary structure estimation revealed the absence of any substantial difference in the secondary structure content (Figure 3B), indicating a specific and different pathway in the protein denaturation due to heating in comparison to that induced by UV exposure.

The melting curve constructed by plotting the ellipticity at 194 nm versus temperature (Figure 3A, inset) showed the presence of two equilibria having T_M values of 21 and 60 °C. The presence of two equilibria reflects the heterogeneity of the WS protein fraction isolated. Moreover, the comparison of the SRCD spectrum recorded at 20 °C during the thermal denaturation assay and that at the end of the heating process showed an evident difference at 216 nm, suggesting that the denaturation process is not completely reversible and that proteins adopted a structure near to the native conformation after heating.

2.4. Fluorescence Spectroscopy. Parallel fluorescence analysis of the WS protein fraction was carried out by recording the fluorescence emission spectra in the 310−550 nm range after selective excitation of the Trp residues at 295 nm. Indeed, these residues play a crucial role in the protective mechanism of lens and retina toward the harmful UV light, dispersing the radiation energy by a fluorescence resonance energy transfer mechanism.[46] Moreover, as demonstrated by the near-UV CD studies, they are dramatically modified by the exposure to UV radiation.

The analysis of fluorescence emission showed that the exposure to UV-C radiation induced both an emission shift to longer wavelengths (Figure S2) and a quenching in the Trp emission (Figure S3). Indeed, the untreated WS protein fraction displays an emission maximum at 338 nm, characteristic of shielded Trp residues, while after exposure to UV light, the Trp emission shifted to 363 nm, characteristic of fully exposed residues.[47] Moreover, the fluorescence intensity decreased as a function of the irradiation time (Figure 4). The most likely mechanism involved in these processes is related to the ROS generation (direct and indirect mechanism previously described) by exposure to UV light as confirmed by experiments on either Ac-Trp-NH_2 (Figure S3) or WS proteins in the presence of ascorbic acid (Figure S5).

2.5. Aggregation of UV-Irradiated Water-Soluble Lens Proteins. The capability of UV-C exposure to induce the aggregation of WS proteins was evaluated determining the

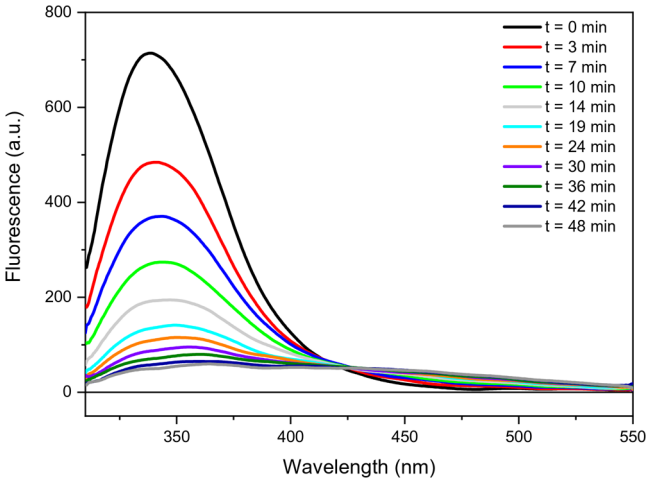

Figure 4. WS proteins fluorescence quenching at increasing irradiation time. Fluorescence spectra were measured as a function of the irradiation time (indicated). WS proteins were 0.025 mg/mL in 10 mM phosphate buffer, pH 7.2. Spectra were recorded at 25 °C using a 10 × 10 mm Suprasil quartz cell on a Perkin Elmer LS50B spectrofluorimeter with excitation at 295 nm, and excitation and emission slit were set at 3.5 nm. Each spectrum is the average of four acquisitions.

aggregation index (A.I.) by UV spectroscopy,[48] analyzing the absorbance at both 350 and 280 nm (Figure S6). As shown in Table S2, the aggregation index (A.I.) increased from 3.5, for the untreated protein, to 25, for the 45 min irradiated protein, indicating the presence of aggregates. This result was confirmed by both electrophoretic and dynamic light scattering (DLS) analyses. Indeed, the electrophoresis of the WS protein fraction after irradiation (Figure 5A), under both reducing and non-reducing conditions, shows that the protein bands corresponding to the crystallin protein monomers disappear, generating high-molecular-weight species, which are so large

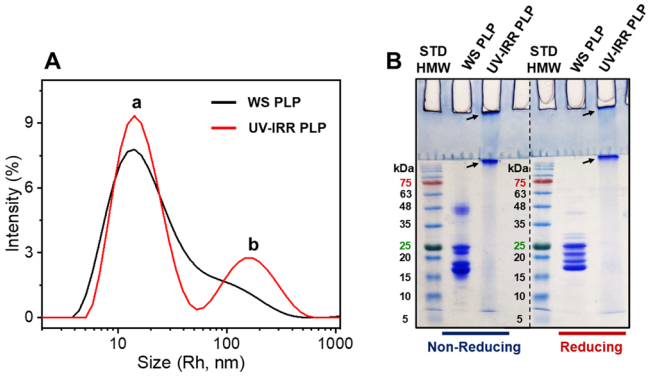

Figure 5. Dimension assessment of untreated and irradiated WS lens proteins. (A) Dynamic light scattering measurements of WS (black solid line) and UV-irradiated (red solid line) porcine lens proteins. All samples (2 mg/mL) were dissolved in 10 mM Tris-HCl buffer, pH 7.2, and equilibrated for 30 min at 25 °C prior to analysis. Data are shown as percent of intensity size distribution. WS PLP, water-soluble pig lens proteins; UV-IRR PLP, UV-irradiated pig lens proteins. (B) SDS-PAGE analysis of WS porcine lens proteins before and after UV-light irradiation, under reducing and non-reducing conditions, as indicated. Arrows indicate very large protein aggregates, which do not enter the running gel or remain in the wells in the stacking gel. STD HMW, high-molecular-weight protein standard mixture.

https://dx.doi.org/10.1021/acsomega.9b04234
ACS Omega 2020, 5, 4293−4301

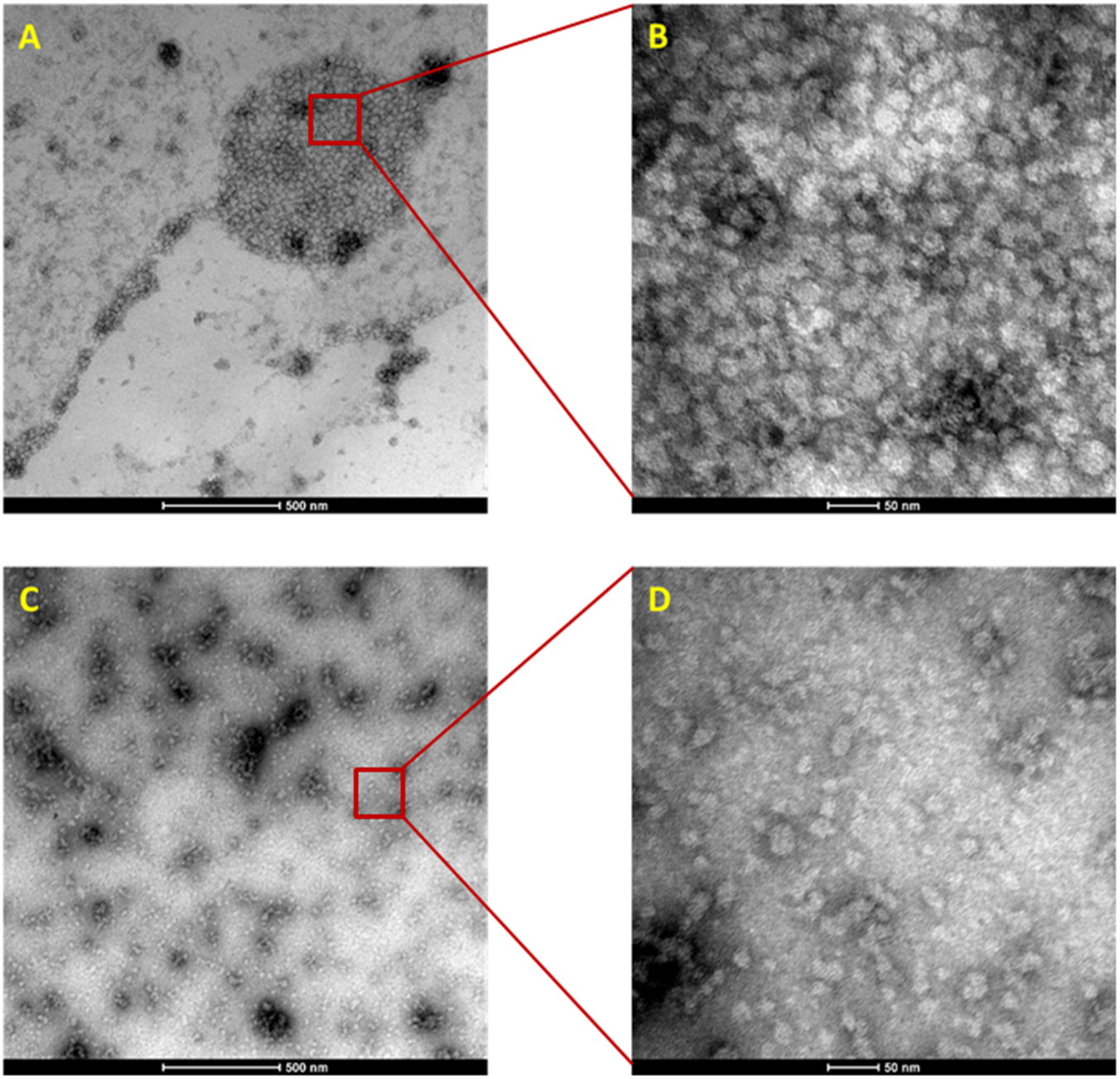

Figure 6. (A, C) Low-magnification and (B, D) medium-magnification TEM images of 50 μM WS lens proteins in 10 mM Tris-HCl buffer, pH 7.2, (A, B) non-irradiated or (C, D) irradiated for 45 min with a 256 nm benchtop UV lamp.

that they are not able to even enter the running gel (12% acrylamide) or remain in the wells in the stacking gel (4% acrylamide), suggesting that the UV light induced the generation of aggregates resistant to the denaturant action of SDS in electrophoretic analysis.

The DLS intensity profile (Figure 5A) of WS proteins before irradiation reveals the presence of a major component having a hydrodynamic radius (Rh) of 14.1 nm and a minor component at 145 nm, both characterized by high % polydispersity (%PD) values (~130%), indicative of high size distribution heterogeneity. These features are compatible with the multimeric state of lens proteins.[6,8] After irradiation, a significant reduction of size heterogeneity was observed (%PD = 48%). However, the major component at Rh = 14.1 nm is still present, along with the minor component that now appears as a distinct peak at 171 nm, suggesting that UV-light irradiation does not alter the size distribution of the non-covalent protein complexes existing under native conditions.

Information on the morphology of protein aggregates were obtained by transmission electron microscopy (TEM) analysis (Figure 6). The untreated sample shows a globular conformation of the WS lens proteins (Figure 6A,B), consistent with literature data.[35] The exposure to UV radiation at neutral pH induced the appearance of amorphous protein aggregates (Figure 6C,D), confirming previous observations and, in particular, the conformational studies (CD and SRCD) that did not show the presence of amyloid structures.

https://dx.doi.org/10.1021/acsomega.9b04234
ACS Omega 2020, 5, 4293−4301

3. CONCLUSIONS

The water-soluble fraction of mammalian lens proteins is composed almost exclusively of α-, β-, and γ-crystallins that contribute to the transparency of the lens providing the refractive index needed to focus light onto the retina. Among the possible causes of protein damage that lead crystallins to aggregate into insoluble clusters causing lens opacification and cataract onset, an important role is represented by the exposure to UV light.

In this paper, the exposure to either UV-C light (254 nm) or far-UV synchrotron radiation in the SRCD photostability assay was used to mimic the effects of UV radiation on WS lens proteins. The major mechanism by which UV and synchrotron radiation induced protein denaturation is the generation of reactive oxygen species by either photolysis of water solvent molecules or excitation of protein chromophores and successive transfer of electron.[44] Our results demonstrated that the conformational changes observed in the WS lens protein fraction following the exposure to UV radiation were mainly due to the action of ROS as confirmed by both the experiments performed in the presence of ascorbic acid, a scavenger of oxygen radicals, and the analysis of tryptic digest of irradiated proteins. Moreover, the denaturation process induced by the exposure to UV light was more efficient than that observed by heating.

These data confirm the possibility to use the crude extract of WS lens proteins containing α-, β-, and γ-crystallins to study the conformational effects of exposure to different crystalline toxic agents. In these conditions, all naturally occurring proteins including α-crystallin whose chaperone-like activity counteracts the misfolding and aggregation of soluble proteins are present. These will be useful to study the ability of small molecules to counteract and protect from damage caused by exposure to both UV light and oxidative stress.

4. MATERIALS AND METHODS

4.1. Pig Lens Protein Extraction. Pig lenses of young healthy animals were provided by a local slaughterhouse and preserved in an antibiotic solution. Lenses, free of irregularities or inclusions, were washed with MilliQ water prior to handling, decapsulated, and then grinded with a bistoury blade, suspended in 5 mM EDTA solution in 10 mM Tris-HCl buffer, pH 7.2, and centrifuged for 20 min at 12000 rpm. The supernatant was filtered on a 0.45 μm nylon filter, aliquoted, and stored at −20 °C. Protein concentration was determined by the Bradford test.[49]

4.2. UV Spectroscopy. UV spectroscopy was performed with a Shimadzu UV-2501 UV−Vis spectrophotometer (Kyoto, Japan). Samples of 1.0 mL were measured in quartz cuvettes (Hellma Analytics, Milan, Italy) with a path length of 10 mm. UV absorbance was recorded from 250 to 500 nm using an integration time of 1.5 s and steps of 0.2 nm. The spectra were processed with UV-Probe software (Shimadzu).

4.3. Fluorescence Spectroscopy. Emission fluorescence spectra were collected using a Perkin Elmer LS50B spectrofluorimeter (Waltham, MA, USA) equipped with FL-WinLab software (Perkin Elmer). Samples were measured in a semi-micro quartz cuvette (10 × 4 mm, Hellma Analytics) thermostated at 25 °C. Emission spectra were recorded from 310 to 550 nm, with excitation at 295 nm, and excitation and emission slits were set at 3.5 nm at a scan speed of 400 nm/min. The spectra were the average of four scans.

Protein denaturation experiments were performed by recording the fluorescence emission spectra of water-soluble lens proteins (0.1 mg/mL) in 10 mM Tris-HCl buffer solution, pH 7.2, irradiated for increasing time with a UV lamp at 254 nm (Spectroline model EF-160C/FE). Data were elaborated using OriginPro 2019 software (Northampton, MA, USA).

4.4. Circular Dichroism. Far- and near-UV CD spectra were measured with a Jasco J-1500 CD spectrometer in combination with a Jasco PTC-423S temperature controller (Jasco International, Tokyo, Japan).

Far-UV CD spectra were collected in quartz cuvettes (Hellma Analytics) with a path length of 1 mm at 25 °C from 185 to 255 nm at a scanning speed of 50 nm/min, a response time of 1 s, a bandwidth of 1 nm, a sensitivity of 200 mdeg, and steps of 0.5 nm. The spectra recorded were the average of nine scans. The protein concentration was 0.09 mg/mL in 10 mM phosphate buffer, pH 7.2.

Near-UV CD spectra were measured in quartz cuvettes (Hellma Analytics) with a path length of 10 mm at 25 °C. The CD spectra were collected from 250 to 360 nm at a scanning speed of 50 nm/min, a response time of 1 s, a bandwidth of 1 nm, a sensitivity of 100 mdeg, and steps of 0.5 nm. The spectra recorded were the average of nine scans. The protein concentration was 0.09 mg/mL in 10 mM phosphate buffer, pH 7.2.

The spectra were subtracted of the buffer spectrum and elaborated using Jasco Spectra Manager (version 1.53.04) and OriginPro 2019 software.

4.5. Synchrotron Radiation Circular Dichroism. Synchrotron radiation circular dichroism experiments were performed at the module B unit at B23 beamline at Diamond Light Source, Harwell Research and Innovation Campus, Didcot, Oxfordshire, UK. SRCD spectra were recorded in the 185−260 nm wavelength range, with 1 s integration time, 1 nm digital resolution, and scan speed of 39 nm/min, using a 0.02 cm Suprasil cuvette (Hellma Analytics). The protein concentration was 0.45 mg/mL in 10 mM phosphate buffer, pH 7.2.

UV-denaturation experiments were performed at 20 °C by recording 30 consecutive repeated scans in the far-UV region using a bandwidth of 1.8 nm. Thermal denaturation experiments were carried out in the 5−90 °C temperature range (increment steps of 5 °C) using a Quantum Peltier temperature controller. Temperature was equilibrated for 5 min before collecting the spectra. The SRCD spectra were recorded in the 185−260 nm wavelength range using a 1.2 nm bandwidth.

The SRCD spectra were subtracted of the buffer spectrum and elaborated using CDApps[50] and OriginPro 2019 software.

4.6. Sample Irradiation. Controlled photodenaturation of samples was performed with a Spectraline EF-160C/FE lamp equipped with one 6 W lamp emitting at 254 nm. The water-soluble lens proteins were irradiated at 0.45 mg/mL concentration solution in a 0.4 cm path length fluorescence quartz cell at a distance of 7.0 cm, and the volume irradiated was about of 4 cm^3. UV absorbance was recorded from 250 to 500 nm according to the described conditions.

The aggregation index (A.I.) was calculated from the UV spectra as $Abs_{350}/(Abs_{280} - Abs_{350}) \times 100$.[48]

4.7. Dynamic Light Scattering. Dynamic light scattering measurements of WS porcine lens proteins samples (2 mg/mL in 10 mM Tris-HCl buffer, pH 7.2) before and after UV irradiation were carried out at 25 °C on a Zetasizer Nano S

https://dx.doi.org/10.1021/acsomega.9b04234
ACS Omega 2020, 5, 4293−4301

(Malvern Instruments, Southborough, UK) using disposable polystyrene cuvettes (8.5 mm light center height, 1 cm path length, and 50 μL) from Sarstedt (Nümbrecht, Germany). Each measurement consisted of a subset of runs automatically determined, 15 s each. Scattering data were analyzed with the Nano-7.12 software and expressed as percentage intensity size distribution, from which the values of hydrodynamic radius (Rh) and % polydispersity (%PD) were extracted.

4.8. Electrophoresis. Native and UV-irradiated WS lens proteins were analyzed by SDS-PAGE (4−12% acrylamide) under either reducing or non-reducing conditions, following the method described by Laemmli.[51] Sample aliquots (5 μL, 10 μg) were added with gel loading buffer solution in the presence or absence of the reducing agent, 2-mercaptoethanol. When reducing conditions were used, protein samples were heated at 95 °C for 5 min. The electrophoretic runs were performed on a Mini-Protean II apparatus (Bio-Rad, Hercules, CA, USA) at 12 mA constant current. BlueElf Prestained Protein Marker (Jena Bioscience, Jena, Germany) was used as protein standard, and the gel was stained with Coomassie Brilliant Blue R250 dye (Saint Louis, MO, USA).

4.9. Protein Digestion and LC−MS/MS Analysis. Samples containing lens soluble proteins, either untreated or UV-irradiated, were digested using sequencing grade modified trypsin (Promega, 12.5 ng/mL in 50 mM NH_4HCO_3) with a substrate-to-enzyme ratio of 1:25 at 37 °C overnight. The mixtures of peptides were then analyzed by LC−MS/MS using a nano-HPLC Ultimate 3000 (Dionex , Thermo Fisher Scientific) interfaced to an LTQ-Orbitrap XL mass spectrometer (Thermo Fisher Scientific). Peptides were loaded onto a NanoEase trap column (Symmetry 300, C18, 5 μm; Waters) with a flow rate of 8 μL/min and then separated using a 11 cm capillary column (PicoFrit 75 μm I.D.; New Objective) packed in-house with C18 material (Aeris Peptide 3.6 μm XB-C18; Phenomenex) using a flow rate of 250 nL/min and a linear gradient of acetonitrile/0.1% formic acid from 3 to 40% in 40 min. Digested proteins (100 ng) from the control sample were analyzed three times under the same analytical conditions.

The instrument operated in a data-dependent mode, with a full scan acquired in the Orbitrap (60,000 resolution) in the 300−1700 m/z range, followed by MS/MS scans of the 10 most intense ions acquired at a lower resolution in the linear ion trap. Three technical replicates were acquired for each of the samples (untreated and UV-irradiated) by analyzing 100 ng of digested proteins under identical chromatographic and analytical conditions.

Raw data files were analyzed with the software Proteome Discoverer (version 1.4; Thermo Fisher Scientific) connected to a Mascot Search Engine server (version 2.2.4; Matrix Science). The search was done against the *Sus scrofa* (pig) section of the Uniprot Database (version 20170130, 26,103 sequences) setting trypsin as a digestive enzyme and a mass tolerance of 10 ppm and 0.6 Da for precursor and fragment ions, respectively. Oxidation of Met, His, Trp, and Pro residues, dioxidation of Trp residues, and protein N-acetylation were set as variable modifications. A search against a randomized database was used by the algorithm Percolator to assess the false discovery rate (FDR). Data were filtered to retain only proteins identified with at least two unique peptides with high confidence (≥99%). Proteins were grouped into protein families according to the principle of maximum parsimony, and a relative quantification of the peptides and proteins between treated and UV-irradiated samples was obtained using the precursor ion area detection node of Proteome Discoverer.

4.10. TEM. About 25 μL of the sample (WS lens proteins, 50 μM in 10 mM Tris-HCl, pH 7.2, non-irradiated or irradiated for 45 min with a 256 nm benchtop UV lamp) was positioned on a 400 mesh film and dyed with a solution of 1% uranyl acetate for 2 min. Samples were observed with a 100 kV Tecnai G2 (FEI) transmission electron microscope. Images were acquired using a Veleta (Olympus Soft Imaging System) digital camera.

■ ASSOCIATED CONTENT

Supporting Information

The Supporting Information is available free of charge at https://pubs.acs.org/doi/10.1021/acsomega.9b04234.

Electrophoretic analysis of WS porcine lens proteins, shift in the λ_{max} emission of Trp in WS pig lens proteins as a function of irradiation time, fluorescence quenching of WS pig lens proteins and of Ac-(L)-Trp-NH_2 as a function of irradiation time, effect of ascorbic acid on the Trp fluorescence emission as a function of irradiation time, UV spectra of WS pig lens proteins as a function of irradiation time, tryptic fragments LC−MS/MS analysis of native and irradiated WS pig lens proteins, and aggregation index values of WS pig lens proteins as a function of irradiation time (PDF)

■ AUTHOR INFORMATION

Corresponding Author

Paolo Ruzza − *Institute of Biomolecular Chemistry of CNR, 35131 Padova, Italy;* orcid.org/0000-0002-5596-9295; Email: paolo.ruzza@unipd.it; Fax: (+)39 049 827 5239

Authors

Claudia Honisch − *Institute of Biomolecular Chemistry of CNR, 35131 Padova, Italy; Department of Chemical Sciences, University of Padova, 35131 Padova, Italy;* orcid.org/0000-0001-9720-6176

Viola Donadello − *Institute of Biomolecular Chemistry of CNR, 35131 Padova, Italy*

Rohanah Hussain − *Diamond Light Source Ltd., Didcot, Oxfordshire OX11 0DE, United Kingdom;* orcid.org/0000-0001-6207-6631

Daniele Peterle − *Department of Pharmaceutical and Pharmacological Sciences, University of Padova, 35131 Padova, Italy*

Vincenzo De Filippis − *Department of Pharmaceutical and Pharmacological Sciences, University of Padova, 35131 Padova, Italy*

Giorgio Arrigoni − *Department of Biomedical Sciences, University of Padova, 35131 Padova, Italy; Proteomics Center, University of Padova and Azienda Ospedaliera di Padova, 35129 Padova, Italy*

Claudio Gatto − *Alchilife Srl, R&D, 35020 Ponte San Nicolò (PD), Italy*

Laura Giurgola − *Alchilife Srl, R&D, 35020 Ponte San Nicolò (PD), Italy*

Giuliano Siligardi − *Diamond Light Source Ltd., Didcot, Oxfordshire OX11 0DE, United Kingdom*

Complete contact information is available at: https://pubs.acs.org/10.1021/acsomega.9b04234

https://dx.doi.org/10.1021/acsomega.9b04234
ACS Omega 2020, 5, 4293−4301

Notes

The authors declare no competing financial interest.

■ ACKNOWLEDGMENTS

This work was carried out with the support of the Diamond Light Source, Beamline B23 (SM-8034 and SM-20210). The research leading to this result has been supported by the project CALIPSOplus under grant agreement 730872 from the EU Framework Programme for Research and Innovation HORIZON 2020.

■ REFERENCES

(1) Campochiaro, P. A. Molecular pathogenesis of retinal and choroidal vascular diseases. *Prog. Retin. Eye Res.* **2015**, *49*, 67−81.
(2) Cheng, W.; Tan, X.; Chen, X. Anatomy and Physiology of the Crystalline Lens. In *Pediatric Lens Disease*; Liu, Y., Ed. Springer: Singapore, 2017; pp 21−28.
(3) Duncan, M. K.; Cvekl, A.; Kantorow, M.; Piatigorsky, J. Lens Crystallins. In *Development of the Ocular Lens*; Lovicu, F. J.; Robinson, M. L., Eds. Cambridge University Press: Cambridge, 2004; pp 119−150.
(4) Richer, S.; Stiles, W.; Zargar, P.; Rezaei, M.; Vo, T.; Bone, R.; Sardi, B. The human lens: A living biometric indicator of health status and successful aging. In *Studies on the Cornea and Lens*; Babizhayev, M. A.; Li, D. W.-C.; Kasus-Jacobi, A.; Žorić, L.; Alió, J. L., Eds. Springer Science+Business Media: New York, 2015, pp 155−186.
(5) Slingsby, C.; Clout, N. J. Structure of the crystallins. *Eye* **1999**, *13*, 395−402.
(6) Delaye, M.; Tardieu, A. Short-range order of crystallin proteins accounts for eye lens transparency. *Nature* **1983**, *302*, 415−417.
(7) Hejtmancik, J. F. The genetics of cataract: our vision becomes clearer. *Am. J. Hum. Genet.* **1998**, *62*, 520−525.
(8) Bloemendal, H.; de Jong, W.; Jaenicke, R.; Lubsen, N. H.; Slingsby, C.; Tardieu, A. Ageing and vision: structure, stability and function of lens crystallins. *Prog. Biophys. Mol. Biol.* **2004**, *86*, 407−485.
(9) Pierscionek, B. K.; Regini, J. W. The gradient index lens of the eye: An opto-biological synchrony. *Prog. Retinal Eye Res.* **2012**, *31*, 332−349.
(10) Bassnett, S.; Shi, Y.; Vrensen, G. F. J. M. Biological glass: structural determinants of eye lens transparency. *Philos. Trans. R. Soc. London, Ser. B* **2011**, *366*, 1250−1264.
(11) Ponce, A.; Takemoto, L. Screening of crystallin-crystallin interactions using microequilibrium dialysis. *Mol. Vis.* **2005**, *11*, 752−757.
(12) Narberhaus, F. Alpha-crystallin-type heat shock proteins: socializing minichaperones in the context of a multichaperone network. *Microbiol. Mol. Biol. Rev.* **2002**, *66*, 64−93.
(13) Markossian, K.; Yudin, I.; Kurganov, B. Mechanism of suppression of protein aggregation by α-crystallin. *Int. J. Mol. Sci.* **2009**, *10*, 1314−1345.
(14) Haslbeck, M.; Peschek, J.; Buchner, J.; Weinkauf, S. Structure and function of α-crystallins: Traversing from in vitro to in vivo. *Biochim. Biophys. Acta - Gen. Subj.* **2016**, *1860*, 149−166.
(15) Mishra, A.; Krishnan, B.; Srivastava, S. S.; Sharma, Y. Microbial βγ-crystallins. *Prog. Biophys. Mol. Biol.* **2014**, *115*, 42−51.
(16) Serebryany, E.; King, J. A. The βγ-crystallins: native state stability and pathways to aggregation. *Prog. Biophys. Mol. Biol.* **2014**, *115*, 32−41.
(17) Hutchinson, E. G.; Thornton, J. M. The Greek key motif: extraction, classification and analysis. *Protein Eng.* **1993**, *6*, 233−245.
(18) Lapatto, R.; Nalini, V.; Bax, B.; Driessen, H.; Lindley, P. F.; Blundell, T. L.; Slingsby, C. High resolution structure of an oligomeric eye lens β-crystallin: Loops, arches, linkers and interfaces in βB2 dimer compared to a monomeric γ-crystallin. *J. Mol. Biol.* **1991**, *222*, 1067−1083.
(19) Vendra, V. P. R.; Agarwal, G.; Chandani, S.; Talla, V.; Srinivasan, N.; Balasubramanian, D. Structural integrity of the Greek key motif in βγ-Crystallins is vital for central eye lens transparency. *PLoS One* **2013**, *8*, No. e70336.
(20) Wistow, G.; Wyatt, K.; David, L.; Gao, C.; Bateman, O.; Bernstein, S.; Tomarev, S.; Segovia, L.; Slingsby, C.; Vihtelic, T. gammaN-crystallin and the evolution of the betagamma-crystallin superfamily in vertebrates. *FEBS J.* **2005**, *272*, 2276−2291.
(21) Hejtmancik, J. F.; Wingfield, P. T.; Sergeev, Y. V. Beta-crystallin association. *Exp. Eye Res.* **2004**, *79*, 377−383.
(22) Kopylova, L. V.; Cherepanov, I. V.; Snytnikova, O. A.; Rumyantseva, Y. V.; Kolosova, N. G.; Tsentalovich, Y. P.; Sagdeev, R. Z. Age-related changes in the water-soluble lens protein composition of Wistar and accelerated-senescence OXYS rats. *Mol. Vis.* **2011**, *17*, 1457−1467.
(23) Kumari, P.; Srinivasagan, R.; Thankappan, B.; Kumarasamy, A. Oxidative stress in applied basic research and clinical practice. In *Studies on the Cornea and Lens*; Babizhayev, M. A.; Li, D. W.-C.; Kasus-Jacobi, A.; Žorić, L.; Alió, J. L., Eds. Springer Science+Business Media: New York, 2015.
(24) Lam, D.; Rao, S. K.; Ratra, V.; Liu, Y.; Mitchell, P.; King, J.; Tassignon, M. J.; Jonas, J.; Pang, C. P.; Chang, D. F. Cataract. *Nat. Rev. Dis. Primers* **2015**, *1*, 15014.
(25) Evans, P.; Wyatt, K.; Wistow, G. J.; Bateman, O. A.; Wallace, B. A.; Slingsby, C. The P23T cataract mutation causes loss of solubility of folded γD-crystallin. *J. Mol. Biol.* **2004**, *343*, 435−444.
(26) Muranov, K. O.; Maloletkina, O. I.; Poliansky, N. B.; Markossian, K. A.; Kleymenov, S. Y.; Rozhkov, S. P.; Goryunov, A. S.; Ostrovsky, M. A.; Kurganov, B. I. Mechanism of aggregation of UV-irradiated β(L)-crystallin. *Exp. Eye Res.* **2011**, *92*, 76−86.
(27) Zorić, L.; Miric, D.; Kisic, B. Basic Review of the Oxidative Stress Role in Age-Related Cataractogenesis. In *Studies on the Cornea and Lens*; Babizhayev, M. A.; Li, D. W.-C.; Kasus-Jacobi, A.; Žorić, L.; Alió, J. L., Eds. Springer Science+Business Media: New York, 2015, pp 147−154.
(28) Young Yoon, S.; Kim, E.; Shin, Y. J. Oxidative Stress in Lens. In *Studies on the Cornea and Lens*; Babizhayev, M. A.; Li, D. W.-C.; Kasus-Jacobi, A.; Žorić, L.; Alió, J. L., Eds. Springer Science+Business Media: New York, 2015, pp 187−207.
(29) Chaudhury, S.; Roy, P.; Dasgupta, S. Green tea flavanols protect human γB-crystallin from oxidative photodamage. *Biochemie* **2017**, *137*, 46−55.
(30) Roskamp, K. W.; Montelongo, D. M.; Anorma, C. D.; Bandak, D. N.; Chua, J. A.; Malecha, K. T.; Martin, R. W. Multiple aggregation pathways in human γS-crystallin and its aggregation-prone G18V variant. *Invest. Ophthalmol. Vis. Sci.* **2017**, *58*, 2397−2405.
(31) Moran, S. D.; Woys, A. M.; Buchanan, L. E.; Bixby, E.; Decatur, S. M.; Zanni, M. T. Two-dimensional IR spectroscopy and segmental ^{13}C labeling reveals the domain structure of human γD-crystallin amyloid fibrils. *Proc. Natl. Acad. Sci. U. S. A.* **2012**, *109*, 3329−3334.
(32) Moran, S. D.; Zhang, T. O.; Decatur, S. M.; Zanni, M. T. Amyloid fiber formation in human γD-Crystallin induced by UV-B photodamage. *Biochemistry* **2013**, *52*, 6169−6181.
(33) Schafheimer, N.; King, J. Tryptophan cluster protects human γD-crystallin from ultraviolet radiation-induced photoaggregation in vitro. *Photochem. Photobiol.* **2013**, *89*, 1106−1115.
(34) Xia, Z.; Yang, Z.; Huynh, T.; King, J. A.; Zhou, R. UV-radiation induced disruption of dry-cavities in human γD-crystallin results in decreased stability and faster unfolding. *Sci. Rep.* **2013**, *3*, 1560.
(35) Meehan, S.; Berry, Y.; Luisi, B.; Dobson, C. M.; Carver, J. A.; MacPhee, C. E. Amyloid fibril formation by lens crystallin proteins and its implications for cataract formation. *J. Biol. Chem.* **2004**, *279*, 3413−3419.
(36) Di Gaspero, M.; Ruzza, P.; Hussain, R.; Vincenzi, S.; Biondi, B.; Gazzola, D.; Siligardi, G.; Curioni, A. Spectroscopy reveals that ethyl esters interact with proteins in wine. *Food Chem.* **2017**, *217*, 373−378.
(37) Hussain, R.; Longo, E.; Siligardi, G. UV-Denaturation assay to assess protein photostability and ligand-binding interactions using the high photon flux of Diamond B23 beamline for SRCD. *Molecules* **2018**, *23*, 1906.

https://dx.doi.org/10.1021/acsomega.9b04234
ACS Omega 2020, 5, 4293−4301

(38) Ruzza, P.; Vitale, R. M.; Hussain, R.; Biondi, B.; Amodeo, P.; Sechi, G.; Siligardi, G. Interactions of GFAP with ceftriaxone and phenytoin: SRCD and molecular docking and dynamic simulation. *Biochim. Biophys. Acta - Gen. Subj.* **2016**, *1860*, 2239−2248.
(39) Whitmore, L.; Wallace, B. A. Protein secondary structure analyses from circular dichroism spectroscopy: Methods and reference databases. *Biopolymers* **2008**, *89*, 392−400.
(40) Brisker-Klaiman, D.; Dreuw, A. Explaining level inversion of the La and Lb states of indole and indole derivatives in polar solvents. *ChemPhysChem* **2015**, *16*, 1695−1702.
(41) Callis, P. R. Transition density topology of the La and Lb states in indoles and purines. *Int. J. Quantum Chem.* **1984**, *26*, 579−588.
(42) Xu, G.; Chance, M. R. Hydroxyl radical-mediated modification of proteins as probes for structural proteomics. *Chem. Rev.* **2007**, *107*, 3514−3543.
(43) Hayyan, M.; Hashim, M. A.; AlNashef, I. M. Superoxide Ion: Generation and Chemical Implications. *Chem. Rev.* **2016**, *116*, 3029−3085.
(44) Pattison, D. I.; Rahmanto, A. S.; Davies, M. J. Photo-oxidation of proteins. *Photochem. Photobiol. Sci.* **2012**, *11*, 38−53.
(45) Ruzza, P.; Vitale, R. M.; Hussain, R.; Montini, A.; Honisch, C.; Pozzebon, A.; Hughes, C. S.; Biondi, B.; Amodeo, P.; Sechi, G.; Siligardi, G. Chaperone-like effect of ceftriaxone on HEWL aggregation: A spectroscopic and computational study. *Biochim. Biophys. Acta − Gen. Subj.* **2018**, *1862*, 1317−1326.
(46) Creed, D. The photophysics and photochemistry of the near-UV absorbing amino acids-I. Tryptophan and its simple derivatives. *Photochem. Photobiol.* **1984**, *39*, 537−562.
(47) Vivian, J. T.; Callis, P. R. Mechanisms of Tryptophan Fluorescence Shifts in Proteins. *Biophys. J.* **2001**, *80*, 2093−2109.
(48) Hawe, A.; Kasper, J. C.; Friess, W.; Jiskoot, W. Structural properties of monoclonal antibody aggregates induced by freeze-thawing and thermal stress. *Eur. J. Pharm. Sci.* **2009**, *38*, 79−87.
(49) Bradford, M. M. A rapid and sensitive method for the quantitation of microgram quantities of protein utilizing the principle of protein-dye binding. *Anal. Biochem.* **1976**, *72*, 248−254.
(50) Hussain, R.; Benning, K.; Javorfi, T.; Longo, E.; Rudd, T. R.; Pulford, B.; Siligardi, G. CDApps: integrated software for experimental planning and data processing at beamline B23, Diamond Light Source. *J. Synchrotron Radiat.* **2015**, *22*, 465−468.
(51) Laemmli, U. K. Cleavage of structural proteins during the assembly of the head of bacteriophage T4. *Nature* **1970**, *227*, 680−685.

https://dx.doi.org/10.1021/acsomega.9b04234
ACS Omega 2020, 5, 4293−4301